Dynamics of podosome stiffness revealed by atomic force microscopy

Anna Labernadie[a,b], Christophe Thibault[b], Christophe Vieu[b], Isabelle Maridonneau-Parini[a,1], and Guillaume M. Charrière[a]

[a]Centre National de la Recherche Scientifique–Institut de Pharmacologie et de Biologie Structurale, Unité Mixte de Recherche 5089, Université de Toulouse, Université Paul Sabatier, F-31077 Toulouse, France; and [b]Centre National de la Recherche Scientifique–Laboratoire d'Analyse et d'Architectures des Systèmes, Université de Toulouse, Université Paul Sabatier, Institut National de Sciences Appliquées, Institut National Polytechnique, Institut Supérieur de l'Aéronautique et de l'Espace, F-31077 Toulouse, France

Podosomes are unique cellular entities specifically found in macrophages and involved in cell–matrix interactions, matrix degradation, and 3D migration. They correspond to a core of F-actin surrounded at its base by matrix receptors. To investigate the structure/function relationships of podosomes, soft lithography, atomic force microscopy (AFM), and correlative fluorescence microscopy were used to characterize podosome physical properties in macrophages differentiated from human blood monocytes. Podosome formation was restricted to delineated areas with micropatterned fibrinogen to facilitate AFM analyses. Podosome height and stiffness were measured with great accuracy in living macrophages (578 ± 209 nm and 43.8 ± 9.3 kPa) and these physical properties were independent of the nature of the underlying matrix. In addition, time-lapse AFM revealed that podosomes harbor two types of overlapping periodic stiffness variations throughout their lifespan, which depend on F-actin and myosin II activity. This report shows that podosome biophysical properties are amenable to AFM, allowing the study of podosomes in living macrophages at nanoscale resolution and the analysis of their intimate dynamics. Such an approach opens up perspectives to better understand the mechanical functionality of podosomes under physiological and pathological contexts.

cytoskeleton | Young's modulus | microcontact printing

Macrophages, which derive from circulating blood monocytes and reside in most tissues, play critical roles in host defense and tissue homeostasis. In case of infections or wounds, macrophages migrate to injured sites and fulfill their functions, but in numerous pathological situations their activities can worsen inflammatory processes. Thus, regulating macrophage migration is being regarded as a promising strategy for the development of anti-inflammatory therapies. Macrophages harbor specialized structures named *podosomes*, which play a pivotal role in migration and matrix degradation (1, 2). As macrophages patrol through a variety of tissues, they encounter a variety of extracellular matrix (ECM) architectures and composition that may influence podosomes formation and organization; however, the extracellular cues that regulate podosome formation and functions remain unclear.

In two dimensions, podosomes appear as unique nanoscale cellular entities anchored into the ventral plasma membrane and perpendicularly oriented from the substratum. They present a core of column-shaped F-actin surrounded at its base by adhesion proteins (i.e., integrins) and actin-binding proteins, including vinculin, talin, and paxillin (3). As shown recently by electron microscopy, podosomes are anchored into a radial F-actin network laying on the ventral membrane that interconnects podosome cores, with their top standing above the rest of this actin network (4, 5). Podosomes are very dynamic structures that present a rapid actin turnover, with a lifespan ranging from 2 to 14 min (6, 7). When macrophages are activated, their podosomes can rearrange in a particular belt-shape structure called a rosette that efficiently degrades the ECM (1, 8). Works on protease-dependent 3D migration of macrophages indicate that podosomes are key elements of this process (1, 9) and correspond to actin-rich protrusive structures invading the ECM (2, 10). Thus podosomes

are probably sites of force generation based on actin polymerization and myosin II activity (11). Although direct quantification of individual podosome forces remains difficult, evaluating podosome biophysical properties would improve our knowledge of their structure/function relationships. Over the last decade, atomic force microscopy (AFM) has been proven to be a powerful tool for the analysis of morphological aspects of cell structures at nanometer scale resolution and more importantly their rheological properties in living cells (12, 13).

Here we combined micropatterned surfaces and AFM to study podosome biophysical properties in human macrophages derived from blood monocytes. Micropatterned ECM proteins revealed that fibrinogen, compared with other matrix proteins, favors podosomes formation. This property was then used to delineate small areas for podosome formation, which was a prerequisite for resolutive AFM investigations. This allowed us to accurately measure podosome height and Young's modulus in different ECM protein contexts. Finally, time-lapse AFM studies of podosome dynamics combined with the use of actin toxins or myosin II inhibitor revealed that this structure exhibits biperiodical Young's modulus oscillations regulated by F-actin dynamics and myosin II activity.

Results

Micropatterned Fibrinogen Polarizes Podosome Formation and Facilitates AFM Analyses. To study podosomes formed on physiologically relevant substrates, we tested different ECM proteins encountered by macrophages in vivo. The percentage of macrophages spread on fibrinogen or fibronectin forming podosomes (≈60%) was significantly enhanced compared with collagen IV or gelatin (≈35%) but similar to naked glass (Fig. S1A). Because fibrinogen is mostly found at inflamed sites, we decided to focus on this protein (14). We started AFM experiments with formaldehyde-fixed macrophages, which allowed the use of correlative fluorescence microscopy. Deflection and topographical images showed the highly textured landscape of macrophages, with membrane ruffles mostly found in podosome-forming regions, as seen at the migration front of polarized macrophages (Fig. 1A). The cells appeared flat, with an average height at the cell periphery of ≈400 nm. Correlative fluorescence microscopy showed that some membrane bumps corresponded to underlying podosomes revealed by F-actin staining (arrowheads, Fig. 1A). However, these observations highlighted that discriminating podosomes in the cell landscape by the use of AFM alone was uncertain, which hindered further analyses. To address this issue, we thought that
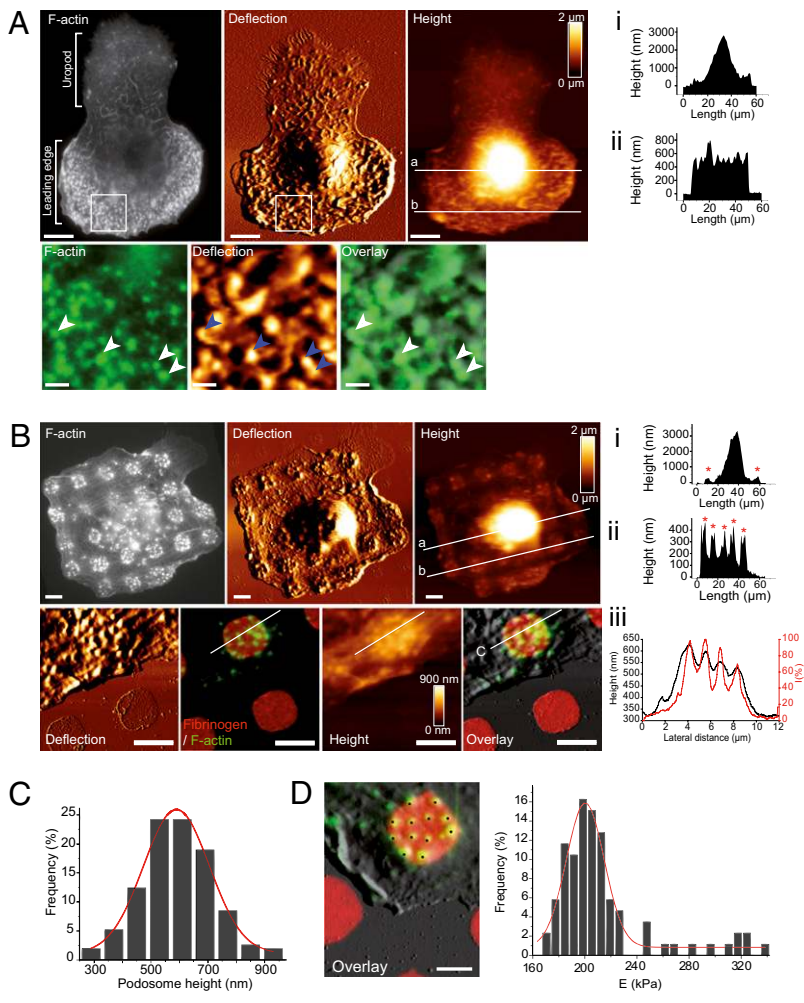
Fig. 1. Macrophage podosomes are amenable to AFM. (*A*) *Upper:* Fluorescence microscopy of F-actin and AFM images of a polarized macrophage after plating on fibrinogen. (Scale bars, 10 μm.) *i* and *ii* correspond to cross-sections (*a* and *b* respectively) extracted from the AFM topographical image to show height profiles. *Lower:* Correlative AFM and fluorescence microscopy: overlay of fluorescence and AFM images are depicted; blue and white arrowheads show emerging bounces corresponding to F-actin dots. (Scale bars, 2 μm.) (*B*) *Upper:* Combined AFM and fluorescence microscopy of a macrophage on micropatterned fibrinogen. Fluorescence staining of F-actin (green) combined with AFM deflection image shows that podosome formation is restricted to protein spots. (Scale bars, 5 μm.) *i* and *ii* correspond to cross-sections (*a* and *b*, respectively) extracted from the topographic image reveal specific areas for podosome formation (red asterisks). *Lower:* Overlay of AFM deflection and fluorescence images of F-actin (green) and fibrinogen spots (red) shows that membrane bumps over fibrinogen spot correspond to podosomes. (Scale bars, 5 μm.) *iii* corresponds to cross-section extracted from the fluorescence and topographic images (line c) shows correlation of fluorescence (red line) and height (black line) signals. (*C*) Height values from AFM topographical images of fixed macrophages on fibrinogen spots harbor a Gaussian distribution (red curve), with a mean of 591 ± 125 nm. (*D*) Single force curves on podosomes from fixed macrophages on a fibrinogen spot. Correlative AFM deflection image of podosomes and fluorescence image of merged F-actin (green) and fibrinogen (red); black dots show the 12 points analyzed located on the F-actin core of podosomes. (Scale bar, 2.5 μm.) Young's modulus was calculated for each podosome using a Hertz model (*SI Methods*). The distribution of Young's modulus values was Gaussian (red curve), with a mean of 201.2 ± 69.8 kPa. Height and Young's modulus measurements were performed on at least 86 podosomes in six cells from three donors.

restricting podosome formation to well-defined areas by using micropatterned matrices would improve AFM analyses.

Over the last decade, micropatterned matrices have been introduced in cell biology to study in greater detail cell–matrix interactions, cell spreading, cell fate, and cell division (15, 16). Arrays of 5 × 5-μm squares spaced by 5 μm of collagen IV, gelatin, fibronectin, or fibrinogen were formed by microcontact printing on glass coverslips, and homogeneity and reproducibility were controlled by AFM (Fig. S1 *B* and *C*). When macrophages were plated on the different micropatterned ECM proteins, striking differences in podosome organization were noticed (Fig. S1*D*). With fibrinogen, 52% of macrophages formed podosomes on protein spots, whereas with the three other proteins most podosomes formed out of the protein spots (Fig. S1*E*). Thus fibrinogen favors formation of podosomes, whereas gelatin and collagen IV repulse them. Therefore, micropatterned fibrinogen was chosen to further study podosomes by AFM. Under these conditions, each membrane bump, clearly noticeable on height profiles (Fig. 1*B*) and present on top of fibrinogen patterns, could be attributed to the F-actin cores of podosomes observed by fluorescence microscopy (Fig. 1*B*). Thus, micropatterned fibrinogen offers multiple benefits by delineating areas of podosome formation, restricting the field size to be analyzed, and reducing the amount of membrane ruffling, rendering podosomes more amenable to AFM.

By using this approach we measured the height of hundreds of podosomes (Fig. 1*C*), validated by correlative fluorescence microscopy (Fig. 1*B* and Fig. S2*A*). The distribution of podosome height values was Gaussian, with an average of 591 ± 125 nm, and

was correlated to their relative F-actin content ($r^2 \approx 0.7$; Fig. S2*B*). When plated on nonpatterned fibrinogen, some macrophages reorganized their podosomes as rosettes. The height of podosome rosettes did not significantly differ from that of isolated podosomes, with an average of 572 ± 119 nm (Fig. S2*C*), suggesting that podosomes have steady height independent of their organization.

Seeking further insight into the structure/function relationships of podosomes, we investigated podosome rheological properties by using AFM as a nanoscale indenter. Force volume mapping of macrophages plated on fibrinogen patterns revealed that podosome-induced membrane bumps in the landscape correlated with pixels of higher stiffness (Fig. S2*D*). Although this approach offers a good overview of podosome stiffness, we chose to improve our analysis by using a force–distance curve approach, which allows a greater accuracy and a faster acquisition for podosome Young's modulus determination. The values of Young's modulus showed a Gaussian distribution, with a mean of 201.2 ± 69.8 kPa (Fig. 1*D*), whereas the average Young's modulus of podosome-free areas in the same cells was 83.8 ± 16.7 kPa, indicating that podosomes are rather stiff structures.

Defining Podosome Physical Properties in Living Macrophages. Because AFM can be operated in near physiological conditions, podosome biophysical properties in living macrophages were investigated on the basis of our work on fixed cells. Time series of AFM topological images on living macrophages (Fig. 2*A* and Fig. S3*A*) showed that podosome height values were homogeneous, with a Gaussian distribution and a mean value of 578 ± 209 nm,
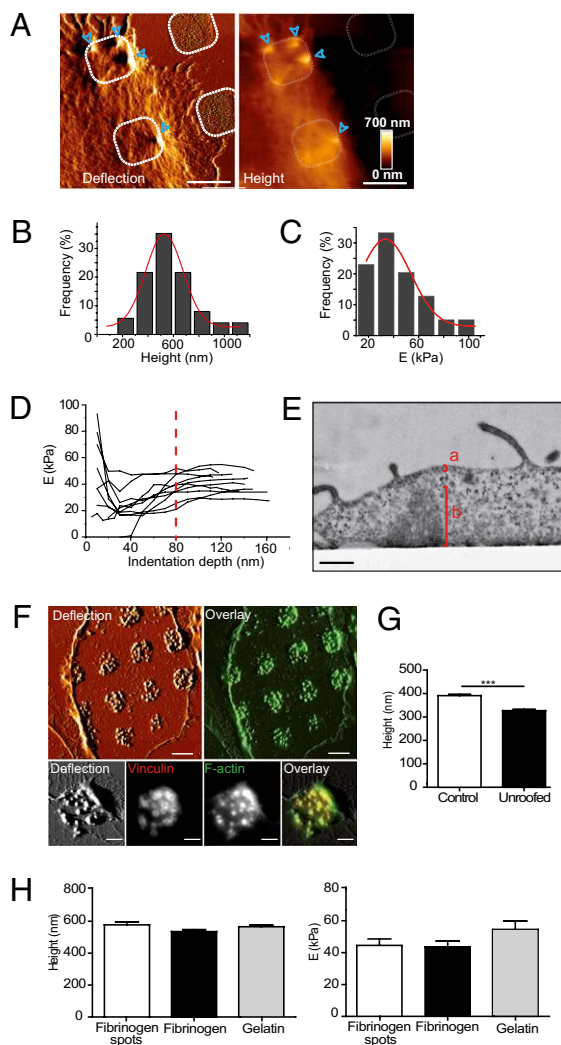
Fig. 2. Biophysical properties of podosomes in living macrophages. (*A*) AFM deflection and topographical images of podosomes on fibrinogen spots. Dotted lines delineate fibrinogen spots underneath the cell, and blue arrowheads show podosomes. (Scale bars, 5 μm.) (*B*) Podosome height values from AFM topographical images of living macrophages on micropatterned fibrinogen exhibited a Gaussian distribution (red curve), with a mean of 578 ± 209 nm (*n* = 125 podosomes in 19 cells from seven donors). (*C*) The distribution of Young's modulus values was Gaussian (red curve), with a mean of 43.8 ± 9.3 kPa (*n* = 39 podosomes in 17 cells from four donors). (*D*) Young's modulus vs. indentation depth of podosomes. Representative curves of different podosomes are displayed (*n* = 10 podosomes in 10 cells from five donors). Dashed line shows the average indentation depth above which the Young's modulus reaches a plateau. (*E*) Transmission electron micrograph of a podosome at the cell periphery: a, dorsal membrane and cortical actin; b, podosome core. (Scale bar, 500 nm.) (*F*) *Upper:* AFM deflection of an unroofed macrophage plated on fibrinogen spots (*Left*) and overlay of AFM deflection combined to fluorescence image (*Right*). *Lower:* Correlative microscopy of AFM deflection and fluorescence images of F-actin and vinculin of an unroofed macrophage. (Scale bars, 2 μm.) (*G*) Quantification of podosome height of control and unroofed macrophages; mean values are 392.5 ± 110 nm and 328 ± 94 nm, respectively. Measurements were performed on at least 392 podosomes in 26 cells from at least four donors for each condition. (*H*) Height and Young's modulus podosomes in macrophages plated for 2 h on fibrinogen spots or nonpatterned gelatin and fibrinogen. Height and Young's modulus were measured on at least 125 podosomes in eight cells and on 17 podosomes in four cells, respectively, from at least two donors for each condition. One-way ANOVA shows that variance is not significant over the tested conditions.

which was comparable to fixed cells (Fig. 2*B*). Moreover, the sequence of AFM images suggested that podosome formation and dynamics (lifespan ≈4 min) are amenable to AFM in living macrophages without disturbing the cells when compared with time-lapse fluorescence imaging (Fig. S3 and Movie S1).

Podosome average Young's modulus in living macrophages was 43.8 ± 9.3 kPa (Fig. 2*C*), which was fivefold higher than that of podosome-free regions (8 ± 1.7 kPa) and lower than in fixed macrophages in which formaldehyde increases biological sample stiffness (17). This value of podosome stiffness was two- to threefold higher than that of stress fibers measured by AFM in other work (12), suggesting that podosome stiffness may reflect specific properties as a matter of composition and/or architecture. Force–distance curves were also analyzed to estimate the thickness of overlying layers crossed by the AFM tip before reaching the top of the podosome core. For this purpose we studied stiffness as a function of indentation depth [as previously performed by Lu et al. on stress fibers (12)]. By postulating that under these conditions F-actin polymer harbors isotropic properties, the Young's modulus value of such polymer would be independent of indentation depth; thus, curves of stiffness as a function of the indentation would reach a plateau when the AFM tip is indenting the F-actin polymer (12). Analysis of multiple force–distance curves showed that the stiffness plateau was reach after the first 80 nm of indentation in all cases, indicating that the thickness of superficial layers crossed by the AFM tip before indenting the podosome F-actin core is ≈80 nm (Fig. 2*D*). To verify the accuracy of this estimation, two complementary approaches were used. First, transmission electron microscopy was performed on transversal sections of macrophages, and second, dorsal membrane was removed by unroofing to gain direct access to podosome cores. Transmission electron microscopy images of the cell periphery showed the proximity between the dorsal plasma membrane and the electron-dense F-actin core of podosomes anchored into the ventral membrane (Fig. 2*E*). The dorsal plasma membrane is supported by a thin cortex of F-actin, with a total thickness (membrane and F-actin cortex) ranging from 60 nm to 80 nm. Thus, the fluid phase of the cytoplasm probably flows out of the region when the AFM tip applies pressure on the plasma membrane. Direct measurement of F-actin core by AFM after cell unroofing showed a difference of 64 ± 7 nm when compared with intact cells. This value corresponded to the thickness of the dorsal membrane and its associated actin cortex that were removed during the unroofing process (Fig. 2 *F* and *G*). In these experiments, intact and unroofed cells were fixed with glutaraldehyde instead of formaldehyde, and this could explain why podosome height values were lower than those measured before. Altogether the three approaches indicated that the AFM tip reaches the top of the podosome F-actin after the first 80 nm of indentation. In our experimental setup, the total indentation depth on podosomes in living macrophages ranged from 120 nm to 170 nm, which ensured that the AFM tip indented the F-actin core of podosomes.

Because podosome formation was modulated differently depending on the nature of the ECM protein (Fig. S1), we wondered whether their physical properties could be influenced by the underlying ECM protein. Podosome height and stiffness on nonpatterned gelatin were compared with fibrinogen patterned or not (Fig. 2*H*), and no significant differences were observed. These results suggest that podosomes have constant structural properties independent of the nature and the organization of the ECM.

Dynamics of Podosome Young's Modulus Revealed by Time-Lapse AFM. F-actin turnover in podosomes has been shown to be highly dynamic (5–7), hence we examined how podosome Young's modulus behaves over their lifespan. The AFM force–distance curves approach was used to track single podosome stiffness dynamics as fast as one measure per second over several minutes.

Fig. 3*A* displays representative deflection and topographical images of a podosome, with its corresponding stiffness over time curve extracted from the successive force curves. Two types of stiffness variation were reproducibly found: first, small and rapid oscillations (average duration 9.8 ± 5.1 s, average magnitude 21.7 ± 9.9 kPa) that we called type I (black curve). Second, larger variations of the average stiffness were found (red curve) and were called type II (average duration 52.9 ± 22.5 s, average magnitude 30.3 ± 20.5 kPa). During these experiments, variations of podosome relative height were estimated from the force–distance curves by considering the offset piezo position and the contact point position calculated from the Hertzian model (*SI Materials and Methods*). Podosome height variations averaged at a magnitude of 55 ± 27 nm, which was considered to be negligible because they represent less than 10% of podosome height (Fig. S4*A*). To verify that podosome stiffness variations were not disturbed by movements of the overlying dorsal plasma membrane, stiffness dynamics of podosome-free regions were examined (Fig. 3*B*). Stiffness variations in such areas greatly differed from podosomes in terms of magnitude (3 ± 0.6 kPa) and duration (6 ± 0.9 s). These results helped us to define a podosome stiffness threshold that was set at 12 kPa (corresponding to the E_{mean} + 2 SD of podosome-free areas; blue line in Fig. 3*B*). As shown in Fig. 3*C*, when podosomes disappeared, a sudden decrease of average stiffness was observed, dropping down to podosome-free area stiffness values, and this was confirmed by the height reduction observed on the topographical image (Fig. 3*C*). The different types of variations encountered over several podosomes are represented as a dot plot (Fig. 3*D*), which highlighted that type I and type II variations segregated differently, even when considering podosome-to-podosome heterogeneity (Table S1). To assess the periodicity of type I and type II variations, Fourier transforms of podosome stiffness over time curves were analyzed. The representative Fourier transforms of a podosome presented in Fig. 3*E* show frequency maxima at 0.14 Hz for type I and 0.031 Hz for type II. These frequencies correspond to periods of 7.1 s for type I and 32.2 s for type II, which are reasonably close to the measured periods (6 s for type I and 32 s for type II). As a control, Fourier transforms of podosome-free regions did not show any periodicity (Fig. 3*E*). Altogether our results reveal that podosomes harbor particular biperiodic stiffness oscillations throughout their lifespan.

Biophysical Properties of Podosomes Reflect F-actin Core Properties and Depend on Myosin II Activity. To determine whether podosome biophysical properties reflect actin-related processes, two actin-targeting toxins, cytochalasin D (CD) and jasplakinolide (Jas), were used. CD is a cell-permeant toxin that inhibits actin polymerization by capping the barbed ends of F-actin filaments and blocking the addition of new G-actin monomers, thus favoring F-actin filament depolymerization and severing (18). Treatment of macrophages with 2 μM CD induced the rapid disruption of F-actin radial network and cortex, but podosome F-actin cores remained (Fig. 4*A*, Figs. S5 and S6*A*, and Movie S2). In accordance with CD affecting F-actin polymerization, podosome height was reduced by 30% (Fig. 4*B*). This effect of CD was confirmed by measuring F-actin core height directly in unroofed macrophages, which was reduced by 33% (Fig. 4 *C* and *D*). In parallel with the height reduction induced by CD, a 50% decrease of stiffness was observed in living macrophages (Fig. 4*B*), showing that the disturbance of F-actin stability profoundly impaired podosome biophysical properties. Jas is a cell-permeant toxin that stabilizes F-actin (19). Cells treated with 250 nM of Jas did not show any
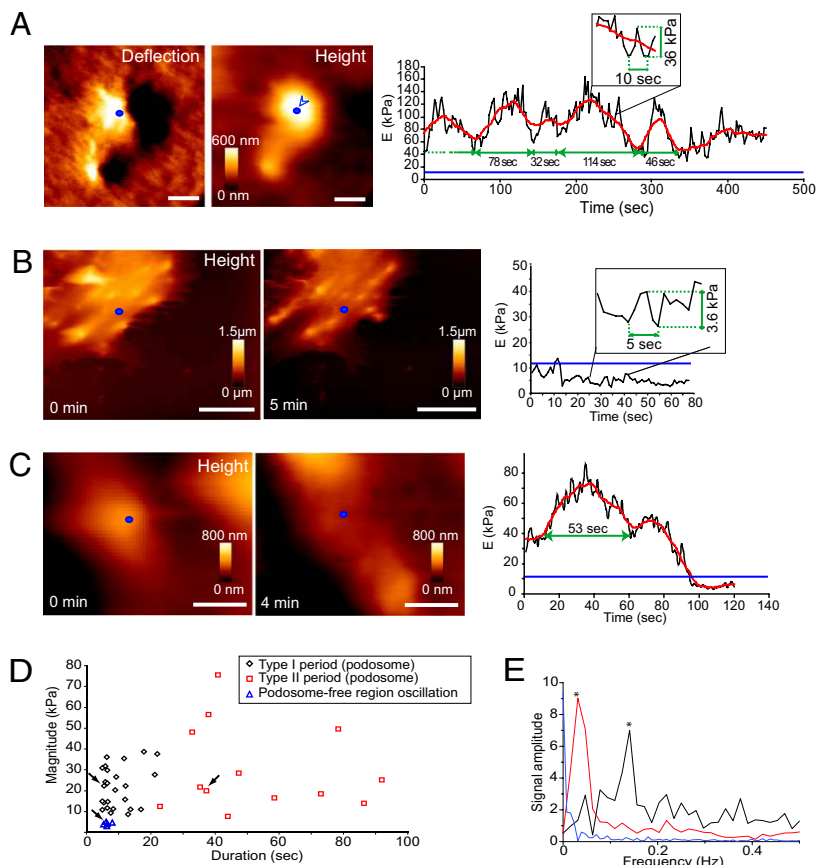
A

B

C

D

E

Fig. 3. Podosome stiffness dynamics measured by time-lapse AFM. (*A*) Young's modulus variations over time of a podosome in a living human macrophage on fibrinogen patterns, with images of its AFM deflection and topography. (Scale bars, 0.5 μm.) Blue dot indicates AFM tip position, and height at this point is 545 nm. *Right:* Curve of stiffness over time obtained by recording a single force–distance curve per second. Black curve corresponds to raw values, with small oscillations of stiffness (type I, *Inset*). Larger variations, type II, were identified on the smoothed curve (red curve). Blue line indicates the threshold of podosome rigidity (12 kPa) calculated from podosome-free region values. (*B*) Young's modulus variations over time of a podosome-free region in a living human macrophage. Images are AFM topography of a podosome-free region before (*Left*) and after (*Center*) the recording of single force curves (*Right*). *Inset:* Magnified part with typical stiffness variations. (Scale bars, 5 μm.) (*C*) Young's modulus variations over time during podosome disruption. Images are AFM topography of a podosome before (*Left*) and after (*C*) the recording of single force curves every second (*Right*). Heights values at the blue point before and after recording are equal to 720 nm and 520 nm, respectively. (Scale bars, 1 μm.) (*D*) Scatter plot of magnitude as a function of duration for type I and type II stiffness variations from podosomes and podosome-free areas. Each dot represents the mean of magnitude and duration in the stiffness dynamics acquired for at least 13 podosomes in 10 cells from three donors for each condition. (*E*) Representative Fourier transforms (FT) of type I (black curve), type II (red curve), and podosome-free regions oscillations (blue curve) of the E (kPa) time series dynamic. *Type I pic$_{max}$= 0.140 Hz; type II pic$_{max}$= 0.031 Hz. Arrows in *D* display the values extracted semi-automatically from the same stiffness dynamics. FT analysis was performed on 10 podosomes and five podosome-free regions stiffness dynamics, as described in *SI Materials and Methods*.
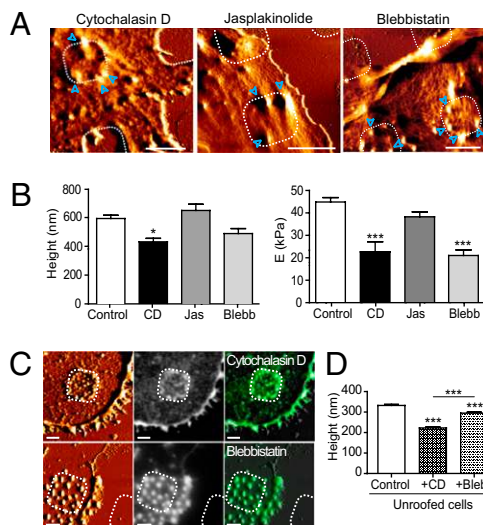
Fig. 4. Effects of cytoskeleton-disturbing drugs on podosome biophysical parameters. (*A*) AFM deflection images of a macrophage treated for 20 min with CD, Jas, or Blebb; blue arrowheads show podosomes. (Scale bars, 5 µm.) (*B*) Height and Young's modulus of podosomes in macrophages; DMSO-treated cells (control) or treated with CD, Jas, or Blebb, up to 60 min. Experiments were performed on at least 14 podosomes in 10 cells from three donors. (*C*) AFM deflection image (*Left*), fluorescence microscopy of F-actin (*Center*), and merge images (*Right*) of an unroofed macrophage treated 20 min with CD or Blebb. (Scale bar, 2 µm.) (*D*) Quantification of podosome height of unroofed macrophages and unroofed macrophages treated with CD or Blebb; mean values are 328 ± 94 nm, 219 ± 89 nm, and 291 ± 87.5 nm, respectively. Values were obtained from at least 260 podosomes in 10 cells from three donors for each condition.

Fig. 5. Effects of cytoskeleton-disturbing drugs on podosome stiffness dynamics. (*A*) Representative Young's modulus variations over time of podosomes in a living human macrophage on fibrinogen patterns before (control) and during treatment with CD, Jas, or Blebb. At least 14 podosomes in 10 cells from three donors were studied for each condition. (*B*) Representative Fourier transform of type I and type II oscillations of the Young's modulus time series dynamic before (control) and during treatment with CD, Jas, or Blebb. Dashed lines indicate type I peak$_{max}$= 0.140 Hz, type II peak$_{max}$= 0.031 Hz. *Artifactual peaks whose value corresponds to the entire recording time.

apparent modifications of their F-actin network (Fig. 4*A*, Figs. S5 and S6*B*, and Movie S3); moreover, there was no modification of podosome height or stiffness (Fig. 4*B*). These results show that our experimental setup provides a direct estimation of the effects of actin toxins on podosome F-actin core.

Cell cytoskeleton architecture and dynamics are mostly regulated by actomyosin complexes as observed during phagocytosis (20). Myosin IIA localizes into F-actin radial network at the vicinity of podosomes (Fig. S5) and has been shown to regulate podosome dynamics (3, 21); therefore, we assessed the role of myosin II activity in the regulation of podosome biophysical properties. For this purpose, macrophages were treated with 50 µM of blebbistatin (Blebb) and analyzed by fluorescent microscopy and AFM. In accordance with previous works (22), myosin IIA localization was profoundly affected by Blebb treatment, whereas most podosomes remained in our conditions (Fig. 4*A* and Fig. S5). AFM experiments showed that Blebb weakly impaired podosome height (confirmed on unroofed cells; Fig. 4*C*) while reducing podosome stiffness by 53% (Fig. 4*B*). Therefore, myosin II does not seem to regulate podosomes architecture per se but tunes their viscoelastic properties, probably by regulating actin filaments tension.

Next the effects of CD, Jas, and Blebb were examined on the dynamical aspects of podosome Young's modulus. At different time points after drug addition, time-lapse AFM data were acquired (Fig. 5*A*). The three drugs markedly affected the magnitude of Young's modulus variations, even though Jas did not show any effect on static analyses. Then, in order to estimate how type I and type II periods were specifically affected in these conditions, Fourier transforms were analyzed (Fig. 5*B*). The periodicity of the type I periods was abolished by the three drugs, whereas type II periods were abolished by CD and Blebb but remained with a reduced magnitude in the presence of Jas. Overall, our results show that the periodicity of podosomes Young's modulus dynamics depends on F-actin integrity, treadmilling, and myosin II activity.
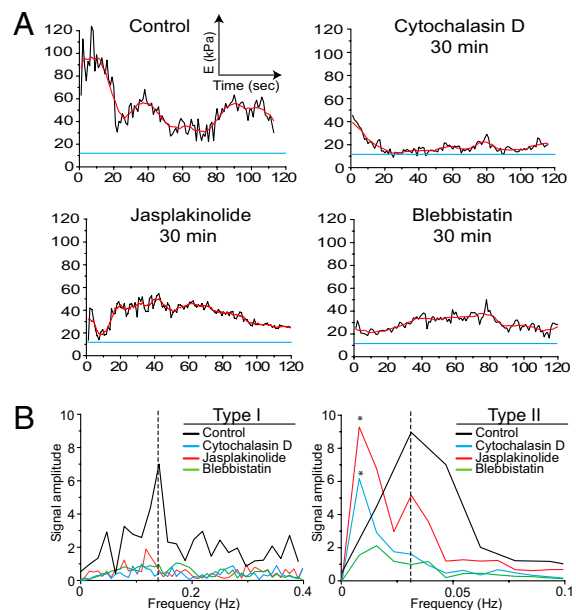
Discussion

In this work, we assessed podosome physical properties by combining the use of AFM, micropatterned surfaces, and correlative fluorescence microscopy. Such a strategy allowed us to perform nanoscale analysis of podosomes in living macrophages, further improving our knowledge of podosome physical aspects and dynamics.

When testing the patterning of different ECM proteins on podosome formation, we observed various effects dependent on protein type and/or patterning. The fact that macrophages responded to micropatterned gelatin by avoiding protein spots to form their podosomes was unexpected because gelatin is commonly used to assess podosome degradative activity. Another interesting result was that fibronectin promoted podosomes formation when nonpatterned, whereas podosomes formed mostly out of the fibronectin spots on micropatterned substrates (compare Fig. S1*A* with Fig. S1*E*). Thus, podosome formation seems to be regulated by the nature and distribution of the ECM protein. However, the comparison of podosome physical properties in different contexts, either in rosette or individualized, or on different ECM proteins showed that podosomes have steady height and stiffness, indicating that they are mostly regulated at the initiation step rather than at their architectural level. Because the ECM proteins used in this study are known to recruit different integrin families—β2 and β3 for fibrinogen, β1 and β3 for fibronectin, and β1 for collagen IV and gelatin (14, 23)—we propose that β2 integrin ligands, here fibrinogen, deliver a strong podosome triggering signal, whereas β1 integrin ligands may have the opposite effect (24). Because podosomes belong to the migration machinery, our results suggest that ECM composition and organization could influence macrophages by defining distinct "functional" zones guiding their migration paths.

In this study AFM is revealed as a versatile tool for the study of multiple parameters at a scale suiting individual podosomes. Delineating podosome formation to small areas by using micro-

patterned fibrinogen was an asset for the use of AFM. We were able to precisely measure height and Young's modulus of hundreds of podosomes and estimate the effects of different drugs that affect F-actin treadmilling and stability, as well as myosin II activity. The three drugs affected podosome properties at different levels: CD affected podosome height and stiffness, Blebb affected podosome stiffness without impairing much podosome height, and Jas had an effect on the stiffness dynamics only. These results highlight that AFM allows a refined analysis of multiple aspects of podosome structure and behavior.

Podosome Young's modulus dynamics show type I and type II overlapping periods, suggesting that at least two different processes coexist. A clear understanding of these phenomena will require future in-depth studies; but meanwhile, some hypothesis may be drawn. The duration of type I variations ($\approx$10–20 s) is in the same range as that of actin turnover in podosomes measured by fluorescence recovery after photobleaching (FRAP) or fluorescence loss In photobleaching (FLIP) ($\tau 1/2 \approx$20 s) (5, 6). The impairment of type I periods by CD and Jas reinforced this hypothesis because both drugs affect actin turnover. Blebb also abolished type I periods, suggesting that microfilament tension regulated by myosin II impacts actin treadmilling, as has been found for other cell structures (25, 26). Type II periods are more profound and durable than type I variations and are also actomyosin-related processes because they were abolished by CD and Blebb and were to a lesser extent affected by Jas. Different observations suggest that these oscillations may result from tangential forces transmitted through the radial F-actin between podosomes, because actomyosin complexes are mostly found in these areas (11). Moreover, CD rapidly disrupted the F-actin radial network, thus disturbing myosin IIA localization (Fig. S5). Finally, although Jas did not disturb much F-actin organization or myosin IIA localization (Fig. S5), it was shown recently that Jas can affect some myosin II functions (27). Altogether this work leads us to propose that F-actin treadmilling and actomyosin complex activities generate periodic forces at podosomes. Because these processes have been proposed to participate in the protrusion of podosomes into the ECM (10, 11), the involvement of their periodicity during macrophage migration remains to be elucidated. Podosome biophysical properties are likely to be coupled with their mechanosensing activity. However, investigation of podosome properties in macrophages plated on soft matrix is challenging as these cells tend to round up and form less podosomes (28). Although the exploration of podosome biomechanics is just beginning, here we show that AFM offers the opportunity to directly quantify biophysical processes in podosomes.

Materials and Methods

Detailed procedures are provided in *SI Materials and Methods*.

Cell Culture. Human monocytes were isolated from blood of healthy donors and differentiated for 7 d into macrophages in the presence of human macrophage colony-stimulating factor.

Atomic Force Microscopy. A NanoWizard II (JPK Instruments) AFM mounted on an inverted optical microscope was used for all experiments. Silicon nitride cantilevers (MLCT-AUHW; Veeco) with a nominal spring constant of 10 pN/nm [corrected using the thermal noise method (29)] were used. All AFM images and measurements were obtained in contact mode in liquid.
AFM height measurements. Fixed cells were analyzed in PBS liquid buffer at room temperature. For AFM analysis of living cells, a temperature-controlled sample holder filled with RPMI Hepes (pH 7.4) buffer as culture media was used.
Elasticity measurements. The determination of the elastic modulus from the force–distance curves was performed using a modified Hertz model (30, 31). During elasticity measurements, force–distance curves were recorded continuously at 2 Hz (1 s per approach–retract force curve).

Statistical analysis. A *t* test or one-way ANOVA analysis with Tukey's multiple comparisons posttest was performed using GraphPad Prism. On each graph, SEs are displayed. Statistical significance is indicated as follows: ***P < 0.001; **P < 0.01; *P < 0.05.

1. Cougoule C, et al. (2010) Three-dimensional migration of macrophages requires Hck for podosome organization and extracellular matrix proteolysis. *Blood* 115:1444–1452 (Blood).
2. Van Goethem E, et al. (2010) Macrophage podosomes go 3D. *Eur J Cell Biol*, in press.
3. Linder S (2009) Invadosomes at a glance. *J Cell Sci* 122:3009–3013.
4. Luxenburg C, et al. (2007) The architecture of the adhesive apparatus of cultured osteoclasts: From podosome formation to sealing zone assembly. *PLoS ONE* 2:e179.
5. Dovas A, et al. (2009) Regulation of podosome dynamics by WASp phosphorylation: implication in matrix degradation and chemotaxis in macrophages. *J Cell Sci* 122:3873–3882.
6. Destaing O, Saltel F, Géminard JC, Jurdic P, Bard F (2003) Podosomes display actin turnover and dynamic self-organization in osteoclasts expressing actin-green fluorescent protein. *Mol Biol Cell* 14:407–416.
7. Evans JG, Correia I, Krasavina O, Watson N, Matsudaira P (2003) Macrophage podosomes assemble at the leading lamella by growth and fragmentation. *J Cell Biol* 161:697–705.
8. Poincloux R, et al. (2006) Re-arrangements of podosome structures are observed when Hck is activated in myeloid cells. *Eur J Cell Biol* 85:327–332.
9. Van Goethem E, Poincloux R, Gauffre F, Maridonneau-Parini I, Le Cabec V (2010) Matrix architecture dictates three-dimensional migration modes of human macrophages: Differential involvement of proteases and podosome-like structures. *J Immunol* 184:1049–1061.
10. Gawden-Bone C, et al. (2010) Dendritic cell podosomes are protrusive and invade the extracellular matrix using metalloproteinase MMP-14. *J Cell Sci* 123:1427–1437.
11. Albiges-Rizo C, Destaing O, Fourcade B, Planus E, Block MR (2009) Actin machinery and mechanosensitivity in invadopodia, podosomes and focal adhesions. *J Cell Sci* 122:3037–3049.
12. Lu L, Oswald SJ, Ngu H, Yin FC (2008) Mechanical properties of actin stress fibers in living cells. *Biophys J* 95:6060–6071.
13. Henderson E, Haydon PG, Sakaguchi DS (1992) Actin filament dynamics in living glial cells imaged by atomic force microscopy. *Science* 257:1944–1946.
14. Flick MJ, Du X, Degen JL (2004) Fibrin(ogen)-alpha M beta 2 interactions regulate leukocyte function and innate immunity in vivo. *Exp Biol Med (Maywood)* 229:1105–1110.
15. Chen CS, Mrksich M, Huang S, Whitesides GM, Ingber DE (1997) Geometric control of cell life and death. *Science* 276:1425–1428.
16. Théry M, et al. (2005) The extracellular matrix guides the orientation of the cell division axis. *Nat Cell Biol* 7:947–953.
17. Burns J, Cuschieri A, Campbell P (2006) Optimisation of fixation period on biological cells via time-lapse elasticity mapping. *Jpn J Appl Phys* 45:2341–2344.
18. Cooper JA (1987) Effects of cytochalasin and phalloidin on actin. *J Cell Biol* 105:1473–1478.
19. Bubb MR, Senderowicz AM, Sausville EA, Duncan KL, Korn ED (1994) Jasplakinolide, a cytotoxic natural product, induces actin polymerization and competitively inhibits the binding of phalloidin to F-actin. *J Biol Chem* 269:14869–14871.
20. Tsai RK, Discher DE (2008) Inhibition of "self" engulfment through deactivation of myosin-II at the phagocytic synapse between human cells. *J Cell Biol* 180:989–1003.
21. Van Helden SF, et al. (2008) PGE2-mediated podosome loss in dendritic cells is dependent on actomyosin contraction downstream of the RhoA-Rho-kinase axis. *J Cell Sci* 121:1096–1106.
22. Kolega J (2006) The role of myosin II motor activity in distributing myosin asymmetrically and coupling protrusive activity to cell translocation. *Mol Biol Cell* 17:4435–4445.
23. Hynes RO (2009) The extracellular matrix: Not just pretty fibrils. *Science* 326:1216–1219.
24. Calle Y, Burns S, Thrasher AJ, Jones GE (2006) The leukocyte podosome. *Eur J Cell Biol* 85:151–157.
25. Kozlov MM, Bershadsky AD (2004) Processive capping by formin suggests a force-driven mechanism of actin polymerization. *J Cell Biol* 167:1011–1017.
26. Hirata H, Tatsumi H, Sokabe M (2008) Mechanical forces facilitate actin polymerization at focal adhesions in a zyxin-dependent manner. *J Cell Sci* 121:2795–2804.
27. Rossier OM, et al. (2010) Force generated by actomyosin contraction builds bridges between adhesive contacts. *EMBO J* 29:1055–1068.
28. Féréol S, et al. (2006) Sensitivity of alveolar macrophages to substrate mechanical and adhesive properties. *Cell Motil Cytoskeleton* 63:321–340.
29. Hutter JL, Bechhoefer J (1993) Calibration of atomic-force microscope tips. *Rev Sci Instrum* 64:1868–1873.
30. Hertz H (1882) Über die Berührung fester elastischer Körper. *J Reine Angewandte Mathematik*, 92:156–171 (in German).
31. Sneddon I (1965) The relation between load and penetration in the axisymmetric boussinesq problem for a punch of arbitrary profile. *Int J Eng Sci* 3:47–57.

CELL BIOLOGY

APPLIED PHYSICAL SCIENCES